Published in final edited form as:
Nat Struct Mol Biol. 2004 June ; 11(6): 567–573. doi:10.1038/nsmb769.

Assembly of endocytic machinery around individual influenza viruses during viral entry

Michael J. Rust[1], **Melike Lakadamyali**[1], **Feng Zhang**, and **Xiaowei Zhuang**[2]
Department of Chemistry and Chemical Biology, Harvard University, Cambridge, MA 02138

Abstract

Most viruses enter cells via receptor-mediated endocytosis. However, the entry mechanisms used by many of them remain unclear. How viruses are targeted to cellular endocytic machinery is also largely unknown. We have studied the entry mechanisms of influenza viruses by tracking the interaction of single viruses with cellular endocytic structures in real time using fluorescence microscopy. Our results show that influenza can exploit clathrin-mediated and clathrin- and caveolin-independent endocytic pathways in parallel, both pathways leading to viral fusion with similar efficiency. Remarkably, viruses taking the clathrin-mediated pathway enter cells via the *de novo* formation of clathrin-coated pits (CCPs) at viral binding sites. CCP formation at these sites is much faster than elsewhere on the cell surface, suggesting a virus-induced CCP formation mechanism that may be commonly exploited by many other types of viruses.

Many viruses infect their host cells via endocytosis. While the endocytic pathways used by some viruses have been determined, the entry mechanisms for most remain poorly understood[1–9]. This is in part due to the presence of multiple endocytic pathways that may be exploited by viruses, including clathrin-mediated endocytosis, caveolin-mediated endocytosis, and clathrin- and caveolin-independent pathways[10–14]. Another important question in viral entry is how viruses are targeted to endocytic machinery for internalization. This is in fact a critical and largely open question for other endocytic ligands as well[11]. For clathrin-mediated endocytosis, ligands and bound receptors are targeted to CCPs, then the CCPs mature into coated vesicles (CCVs), resulting in the internalization of ligands and receptors. Two different targeting mechanisms may be possible: 1) ligands and bound receptors may be targeted to pre-existing CCPs on the cell surface, 2) clathrin and cofactors may be recruited to the site of the bound ligand, leading to *de novo* formation of a CCP at that site. So far, only the first mechanism has been directly observed[15,16], by detecting single CCPs in living cells[17]. A direct observation of the second scenario may be more challenging as it requires the real-time detection of single ligand molecules or particles simultaneously with single CCPs.

Because of its medical importance, influenza has long been used as a model system to understand viral entry mechanisms. Influenza viruses enter cells via receptor-mediated endocytosis and then progress to late endosomes where viral fusion leads to the release of the viral genome[1,9,18–23]. While it has been established that influenza binds to the terminal sialic acid of glycoproteins and glycolipids on cell surfaces[18], little is known about how these viruses are targeted to cellular endocytic structures after binding.

The exact endocytic pathway exploited by influenza is also unclear. Electron microscopy of virus infected cells has revealed influenza viruses inside CCPs and CCVs as well as inside

2To whom correspondence should be addressed, E-mail: zhuang@chemistry.harvard.edu.
1These authors contributed equally to this work

smooth pits and vesicles[1], while Semliki Forest viruses were only found to associate with coated structures[24]. However, without real-time imaging, it is not clear whether these smooth pits lead to influenza entry, nor is it known whether the smooth virus-bearing vesicles result from uncoating of CCVs or from clathrin-independent endocytosis. A recent study shows that dominant negative mutants and drugs that specifically block clathrin-mediated and caveolin-mediated endocytosis do not significantly affect the infectivity of influenza[8]. This indicates that the virus can infect cells via a clathrin- and caveolin-independent pathway(s) although it is unclear whether this pathway is utilized by influenza under unperturbed cellular conditions. The relative significance of the clathrin-mediated and clathrin- and caveolin-independent pathways in influenza infection is at present unknown. The molecular mechanism of the clathrin- and caveolin-independent pathway also remains largely elusive.

In this work, we have used real-time fluorescence microscopy to simultaneously track individual influenza viruses and endocytic structures in living cells. This has allowed us to characterize the endocytic mechanism exploited by each virus without inhibiting specific endocytic pathways. In addition, the ability to monitor individual viruses in real time provides previously unavailable information about the dynamics of endocytic processes and is particularly well suited to address how viruses are targeted to endocytic machinery. Our single-virus studies show that influenza viruses enter cells via multiple endocytic pathways, with both the clathrin-mediated pathway and a clathrin- and caveolin-independent pathway(s) significantly populated. Both pathways lead to viral fusion with intracellular membrane compartments and thus, presumably, to the release of the viral genome. Simultaneous tracking of single viruses and single CCPs show that viruses exploiting the clathrin-mediated pathway are internalized via the *de novo* formation of CCPs around the viruses. We have resolved the formation and disassembly dynamics of these CCPs/CCVs in real time. Remarkably, the CCP formation rate is much higher at the sites of bound viruses than elsewhere on the cell surface. The kinetics of CCP formation at these sites suggest that the formation is most likely induced by viral binding.

RESULTS

Imaging endocytic structures and viruses

To visualize endocytic structures in cells, we express clathrin or caveolin fused to fluorescent proteins following previously established procedures[7,17,25,26]. Briefly, we constructed a plasmid encoding enhanced yellow fluorescent protein (EYFP) attached to clathrin light chain a (LCa). This fusion protein was expressed in BS-C-1 cells. It has been shown previously that the functional integrity of clathrin is not compromised by fluorescent protein labels[17,25,27,28]. The distribution of EYFP-labeled clathrin (EYFP-clathrin) in cells shows discrete, dynamic fluorescent structures (Fig. 1, Supplementary Video 1). To test whether the EYFP image reveals all CCPs and CCVs, we have immunolabeled these structures with an antibody against the AP2 complex, an abundant protein in CCPs and CCVs. Over 97% of discrete structures in the immunofluorescence image colocalize with those in the EYFP image (Fig. 1c)[17,25]. In addition, we have imaged fluorescently-labeled transferrin, a known marker for clathrin-mediated endocytosis, and found that over 96% of transferrin spots colocalize with EYFP-clathrin structures before their internalization (Fig. 1d). These spots were subsequently internalized as indicated by microtubule-dependent movement and disappearance of the associated EYFP-clathrin signal (data not shown). These observations suggest that our EYFP fluorescence images reveal nearly all CCPs and CCVs in living cells.

Similarly, we expressed enhanced green fluorescent protein (EGFP)-tagged caveolin-1 (caveolin-1-EGFP) in BS-C-1 cells[7,26,29,30]. The distribution of caveolin-1-EGFP in cells shows discrete fluorescent structures (Supplementary Video 2), which were previously suggested to be individual caveolae and caveosomes[7,26,29,30]. Nearly perfect colocalization

has been found between the caveolin structures in the EGFP image and those in the immunofluorescence image obtained using anti-caveolin antibodies (data not shown)[7]. The cholera toxin subunit β, a known marker for caveolin-mediated endocytosis[31], was successfully internalized via labeled caveolae in these caveolin-1-EGFP expressing cells (Supplementary Fig. 1), indicating that the EGFP label did not significantly perturb the internalization of caveolae[7].

To visualize individual viruses in living cells[32–36], we labeled the influenza virus with a lipophilic dye, DiD. This dye-labeling does not affect viral infectivity[36]. Tracking single viruses revealed a three-stage active transport process (Fig. 2) similar to what we have observed previously in CHO cells, with stage I being an actin-dependent movement in the cell periphery, stage II being a rapid, unidirectional movement on the microtubule towards the perinuclear region, and stage III being a bi-directional, microtubule-dependent movement[36]. The actin- or microtubule-dependence of these movements were tested with actin- or microtubule-disrupting drugs in ways similar to our previous study[36]. Here we use the onset of the microtubule-dependent stage II movement to indicate that internalization of the virus has already occurred. We then determine the endocytic mechanism responsible by examining the colocalization of the virus with CCPs and caveolae prior to this movement.

Multiple influenza entry pathways

To determine whether influenza viruses are internalized via clathrin-mediated endocytosis, we infected BS-C-1 cells expressing EYFP-clathrin with DiD-labeled viruses and imaged individual viruses and clathrin-coated structures simultaneously (Supplementary Video 1). We found that most viruses had been internalized into the cells as indicated by the onset of stage II movement. The average time between viral binding and stage II movement is about 5.6 min, in quantitative agreement with that obtained in cells not expressing EYFP-clathrin[36]. About 65% of the internalized viruses had associated with a discrete clathrin-coated structure for an extended period of time, followed by a rapid disappearance of the clathrin signal (Fig. 2a,b, Supplementary Videos 3 and 4), suggesting the internalization of the viruses via CCPs and the rapid uncoating of CCVs afterwards. The remaining 35% of the viruses did not show any association with clathrin-coated structures before stage II movement (Fig. 2c, Supplementary Video 5), suggesting their internalization via a clathrin-independent pathway. Similar partition values were obtained for infection started at various times ($\geq$ 24 hours) post-transfection with EYFP-clathrin and for infection in cells stably expressing EYFP-clathrin. This partition was also independent of the excitation laser intensity used. The same partition ratio was obtained when we used the initial acidification of virus particles to pH 6[36], instead of stage II movement, as an indication that they have already been internalized into intracellular endocytic compartments (data not shown).

De novo formation of CCPs around viruses

For those viruses endocytosed via the clathrin-mediated pathway, an interesting question arises as to how these viruses are targeted to CCPs. Our quantitative analysis shows that only 6% of the viruses joined with a pre-existing CCP. The remaining 94% were internalized via the *de novo* formation of a CCP at the virus-binding sites: these viruses initially bound to sites that showed no discrete EYFP-clathrin signal and then a fluorescent EYFP spot appeared centered on the virus, typically 2–3 minutes after viral binding. The EYFP fluorescence intensity gradually increased and then rapidly disappeared before the virus started stage II movement (Fig. 2a,b, Supplementary Videos 3 and 4). Our quantitative analysis of the relative displacement between the CCP and the virus confirms this visual impression that CCP formation begins directly centered on the virus (Supplementary Fig. 2). We occasionally observed clathrin-structures passing by, temporarily colocalizing with and then separating from viruses. These events are not counted as clathrin-mediated endocytosis.

Dynamics of clathrin-mediated endocytosis

Real-time observation of the entire formation and disassembly process of CCPs/CCVs around the viruses allows us to determine the dynamics of the process (Fig. 3). The formation of CCPs is initiated on average 190 s after the viruses bind to the cell (Fig. 3a). The probability of CCP formation increases with time initially and peaks after a lag of 170 s following viral binding (Fig. 3a). The clathrin signal persists for about 70 s on average (Fig. 3b). This period includes a clathrin accumulation phase with a roughly linearly increasing clathrin intensity that indicates the recruitment of clathrin to form a CCP, which then pinches off from the plasma membrane to form a CCV, followed by rapid uncoating of the CCV that is typically completed in only a few seconds (Fig. 3b). The lifetimes of the virus-bound CCPs are similar to those of the constitutive CCPs not associated with viruses (data not shown).

The above results show that the viruses were not typically targeted to pre-existing CCPs, but were predominantly internalized via CCPs that formed *de novo* at the site of the bound viruses. However, this does not necessarily imply that the formation of these pits is induced by viral binding. As CCPs are constitutively forming on the cell surface, the possibility exists that a CCP would by chance form at the virus site. To address this possibility, we analyzed the formation rate of CCPs at random sites on the cell surface. Remarkably, we found that the formation rate at random sites was 20 times lower than that at the sites of bound viruses.

Is it then possible that the viruses are captured by “hot spots” on the cell surface that have a higher CCP formation rate[17,25]? To look for these hot spots, we chose sites of pre-existing CCPs and analyzed the waiting time for another CCP to form at the same or nearby sites after the initial CCP had disappeared. The CCP formation rate obtained at these sites is, however, similar to the rate obtained at random sites on the cell surface. Only at less than 5% of the pre-existing-CCP sites, did we observe a rapidly ‘blinking” fluorescent spot that may indicate repetitive CCP formation[17,25]. In addition, the “dark” times at these “blinking” sites are only about 10–20 s, much shorter than the average time it takes for a CCP to appear at a virus binding site both before and after the viral binding event. These results indicate that the *de novo* CCP formation at the virus-binding sites are not due to static “hot spots” on the cell surface.

The possibility remains that the observed high CCP formation rate is due to preferential association of viruses with mobile “hot spots” that have a higher CCP formation rate. If the viruses were indeed internalized by binding to these hypothetical “hot spots” and did not influence the CCP formation rate there, then the probability that a CCP appears at these sites should be independent of time relative to viral binding and the distribution of the relative time (T_1) between viral binding and CCP formation should follow an exponential decay without any lag. This is inconsistent with our observed T_1 distribution, which shows a significant lag (Fig. 3a). Could the lag be caused by the relative movement between viruses and “hot spots” on the cell surface before their association? If so, the average time it takes a CCP to appear at the “hot spots” should be less than $<T_1>$ (190 s). Considering that the average duration of a CCP is 70 s, the probability of finding a CCP at the “hot spots” should be greater than 27% at any time. Thus if viruses move to the “hot spots” to get internalized, the fraction of viruses that joined with a pre-existing CCP should be greater than 27%, again inconsistent with our observed value (6%). These results suggest that the CCPs that appear *de novo* at the sites of the bound viruses are most likely induced or influenced by viral binding.

After clathrin uncoating, the viruses show heterogeneous transport dynamics. The majority of viruses started their microtubule-dependent movement less than 40 s after uncoating; whereas the rest remained in the cell periphery for several minutes before stage II movement (Fig. 3c and Supplementary Fig. S3). For the latter fraction of viruses, the relatively long lag between clathrin uncoating and stage II movement leaves open the possibility that the viruses were recycled back to the cell surface and were then re-endocytosed. Indeed, we occasionally

observed a second round of CCP formation during that period. If the hypothetical re-endocytosis events occur via a clathrin-independent mechanism, it could lead to a moderate effect on the partition ratio of viruses between the clathrin-dependent and -independent pathways, as we detail in Supplementary Fig. 3.

Effect of neuraminidase on influenza entry

Influenza viruses bind to sialic acids on cell surfaces via hemagglutinin in a highly multivalent manner. Such multivalent binding could restrict viral mobility on the cell surface. Influenza neuraminidase cleaves hemagglutinin-sialic acid bonds[37]. It is thus possible that neuraminidase activity facilitates viral movement on the cell surface and targeting to endocytic sites and, therefore, plays a significant role in cellular entry of influenza. However, our observation of *de novo* CCP formation at viral binding sites suggests that neuraminidase activity may not be critical for the internalization of influenza. To test this, we investigated the cellular entry of influenza in the presence of neuraminidase inhibitors RWJ-270201 and Oseltamivir[38,39]. While these inhibitors effectively block influenza infection at the concentration of a few nM (data not shown)[38,39], we fail to observe their effect on viral endocytosis, trafficking and fusion even at 1μM concentration. The relative time between viral binding and the stage II movement is very similar to that in the absence of drugs (Fig. 4), suggesting that neuraminidase is not essential for the cellular entry of influenza and these recently developed influenza drugs function to block other stages of the infection[37].

Clathrin- and caveolin-independent pathway

Next, we address the internalization mechanism of those viruses that entered cells without colocalization with CCPs. To this end, we infected BS-C-1 cells expressing caveolin-1-EGFP with DiD-labeled viruses and imaged individual viruses together with caveolae and caveosomes (Supplementary Video 2). We found that most viruses had been internalized into the cells as indicated by the onset of stage II movement and the average time between viral binding and stage II movement was similar to that in cells not expressing caveolin-1-EGFP. Among the internalized viruses, less than 5% showed co-localization with caveolae/caveosomes before internalization. In cells treated with filipin (5 μg/ml), an inhibitor of caveolin-mediated endocytosis[40], we observed a similar partition ratio of viruses between the clathrin-dependent and -independent pathways to that in untreated cells, while the same filipin treatment blocks the internalization of cholera toxin subunit β [M.L., M.J.R., X.Z. unpublished]. The above observations indicate that the clathrin-independent endocytic pathway exploited by influenza is also caveolin- and lipid raft-independent[14].

To initiate infection, influenza viruses release their genome into the cytoplasm by fusing with endosomes[1,9,18–23]. We tested whether the clathrin-mediated pathway and clathrin- and caveolin-independent pathway both lead to viral fusion. To this end, we labeled the viruses with a high surface density of DiD such that its fluorescence is partially quenched. Viral fusion events can be identified by a dramatic increase in the DiD fluorescence intensity due to fusion-induced dequenching (Fig. 5, Supplementary Videos 6 and 7)[36]. Among the viruses that fused, 69% had shown association with clathrin-coated structures before stage II movement, whereas 31% had not. This partition is almost identical to that obtained for all viruses showing microtubule-dependent movement.

Next, we compare the trafficking kinetics of viruses along the clathrin-dependent and -independent pathways. The distributions of time between viral binding and stage II movement are similar for the two pathways (Supplementary Fig. 4a). This is not surprising if the two endocytic pathways are competing for viral entry. The time distributions between stage II movement and viral fusion are also similar for the two pathways (Supplementary Fig. 4b). This may in part be caused by the convergence of clathrin-mediated and clathrin-independent

pathways in post-endocytic trafficking[41]. We have indeed observed merging events of virus-containing vesicles internalized via the two pathways prior to viral fusion. These results are consistent with a previous finding that influenza viruses enter endosomes at similar times whether or not dominant negative mutants were present to block clathrin-mediated endosytosis[42]. The distances between the fusion sites and the nuclear envelope are also similar for viruses entering via the two pathways (Supplementary Fig. 4c).

The above results indicate that the clathrin-mediated and -independent pathways are equally efficient for viral fusion once the viruses are internalized. Considering previous results that influenza viruses fuse with endosomes to release their genome and initiate infection[1,9,18–23] and that influenza infects cells in the presence of drugs and mutants that block clathrin- and caveolin-mediated endocytosis[8], our data suggest that the two pathways are likely equally efficient for infection once the viruses are internalized. Our results further show that clathrin- and caveolin-independent endocytosis is not an alternative means exploited by influenza only when clathrin-dependent endocytosis is blocked, but a parallel pathway that influenza takes under normal cellular conditions.

DISCUSSION

While receptor-mediated endocytosis is known to be one of the major mechanisms that viruses exploit to enter cells, the molecular mechanisms underlying the complex processes of viral endocytosis are still poorly understood. In this work, we have visualized single influenza viruses and endocytic structures in living cells and tracked the interaction between them in real time using fluorescence microscopy. This has allowed us to determine the endocytic mechanisms exploited by influenza without inhibiting specific endocytic pathways and to directly address how influenza viruses are targeted to endocytic machinery for internalization.

Our single-virus trajectories show that influenza viruses enter cells via multiple endocytic pathways. In any given infection experiment, roughly two thirds of the viruses enter cells via clathrin-mediated endocytosis and the remaining via a clathrin- and caveolin-independent endocytic pathway(s). Both pathways lead to viral fusion with intracellular membrane compartments with a similar efficiency.

By tracking the interaction between viruses and CCPs in real time, we show that the viruses exploiting the clathrin-mediated pathway are predominantly (94%) internalized via *de novo* formation of CCPs around the viruses. While recruitment to pre-existing CCPs has been observed previously for G-protein coupled receptors[15,16], the *de novo* formation of CCPs at the sites of bound ligands has not been directly observed before. We have resolved the dynamics of CCP formation around the viruses: clathrin begins to appear at the viral binding sites a few minutes after binding; this is followed by a roughly linear increase in the clathrin intensity for about one minute, during which time a CCP is formed and matures into a CCV. Immediately after the clathrin intensity reaches its maximum, the clathrin coat rapidly disassembles, typically in only a few seconds. Remarkably, we found that the formation rate of CCPs was 20 times higher at the sites of bound viruses than elsewhere. The formation kinetics of CCPs at these sites suggest that the formation is most likely induced by viral binding.

Ligand-induced clathrin-redistribution to the plasma membrane has been previously reported for epidermal growth factor (EGF) and nerve growth factor (NGF)[43]. There, the binding of EGF to its receptor causes phosphorylation of the clathrin heavy chain and a global redistribution of clathrin to the cell periphery to form CCPs[44]. The majority of newly induced CCPs do not actually colocalize with the NGF receptors[45,46]. This is distinct from our observations of *de novo* formation of CCPs at the virus binding sites without a global redistribution of clathrin upon viral binding.

An interesting question arises: since influenza viruses bind to sialic acids of general glycolipids and glycoproteins on the cell surface instead of specific receptors with known internalization motifs, how is the signal of viral binding transmitted across the plasma membrane to initiate the recruitment of clathrin and associated factors and induce the formation of a CCP at the binding site? One possible mechanism stems from the highly multivalent binding of influenza to the cell via multiple hemagglutinin-sialic acid bonds. This highly multivalent binding of the nearly spherical virus to the cell surface may induce local curvature on the plasma membrane, thereby promoting formation of a CCP at the binding site. It is particularly interesting to note the most conserved domain (BAR domain) of amphiphysin, a component of CCPs, forms a crescent-shaped dimer structure that preferentially binds to highly-curved negative-charged membranes[47]. While the wildtype amphiphysin can efficiently recruit clathrin to liposomes and polymerize clathrin into an invaginated lattice on a lipid monolayer, an amphiphysin with mutations in the BAR domain lacks such ability[47]. We speculate that amphiphysin or other proteins with a similar BAR domain preferentially bind to the curved plasma membrane at the influenza virus binding sites and promote CCP formation at those sites.

METHODS

Viruses and fluorescent labeling

Influenza virus X-31 was purchased from Charles River Laboratories. To label with lipophilic dyes, the viruses were incubated with DiD (Molecular Probes) for 2 hours at 22°C. Unbound dye was removed by buffer exchange into 50 mM HEPES buffer (pH 7.4, 145 mM NaCl) using gel filtration columns. Immediately before experiments, viral aggregates were removed with 0.2 μm pore size filters.

Cell culture

BS-C-1 cells were maintained in a 5% CO_2 environment in Minimum Essential Eagle Medium (MEM, Invitrogen) with 10% (v/v) fetal bovine serum (FBS) and passaged every 2–3 days. For fluorescence imaging, BS-C-1 cells were cultured in MEM with 10% (v/v) FBS in Petri dishes with glass coverslips on the bottom. Prior to fluorescence experiments, cells were washed in serum-free, phenol red-free medium fortified with 100 mM pH 8.0 Hepes buffer.

Plasmids

We obtained the GFP-clathrin-LCa construct as a gift from J. H. Keen[17]. From this construct, the clathrin LCa cDNA was PCR amplified to introduce an *Xho* I restriction site at the 5′ end and an *Age* I restriction site at the 3′ end. Similarly, we amplified the EYFP cDNA, introducing an *Xho* I restriction site at the 3′ end. The EYFP PCR product was cloned into the pcDNA3.1/V5-His-TOPO vector (Invitrogen). This construct was then digested with *Age* I and *Xho* I (New England Biolabs), and the clathrin-LCa PCR product was ligated using the these sites into the vector containing EYFP, yielding a cDNA coding for a chimeric protein with EYFP fused to the N-terminus of clathrin-LCa. The caveolin-1-EGFP construct was a gift from A. Helenius[7].

Transfection of cells

Cells were transfected with EYFP-clathrin-LCa or caveolin-1-EGFP using FuGENE 6 transfection reagent (Roche). For a 60 mm petri dish to be transfected, 2 μl of FuGENE 6 reagent was combined with MEM and 1 μg of DNA for a final volume of 100 μl. The FuGENE/DNA mixture was incubated at room temperature for 20 min, added to the cell culture, and then incubated in 5% CO_2 environment.

Cells stably expressing EYFP-clathrin

The stable cell line was created using the RetroMax retroviral expression system (Imgenex). The EYFP-LCa gene was cloned into the *Hin*d III/*Cla* I restriction sites of the pCLNCX retrovirus expression vector (Imgenex) that confers G418 resistance. 293T cells, growing in Dulbecco's Modified Eagle's Medium (DMEM) containing 10% (v/v) FBS, were then transfected using this vector and the pCL-10A1 retrovirus packaging vector (Imgenex). 293T supernatant was collected after 2 days and filtered through 0.45 micron pore size filters. The target BS-C-1 cells were then infected with an equal volume mix of the 293T supernatant with cell medium (MEM containing 10% (v/v) FBS). 24 hours after infection, the cells were split into various dilutions (1:20 to 1:100) and selection was begun by adding medium containing 1.15 mg ml^{-1} G418. New medium containing G418 was then introduced every three days. Visible antibiotic resistant colonies were formed approximately 14 days after infection. These colonies were then picked and seeded onto new plates and propagated.

Immunofluorescence

Cells transfected with EYFP-clathrin-LCa were fixed in 2% (v/v) formaldehyde for 40 min. After washing with PBS, cells were permeablized in PBS containing 10% (v/v) FBS, 3% (w/v) bovine serum albumin (BSA) and 0.5% (v/v) triton-X 100, and then incubated at 4°C overnight with the monoclonal antibody against α-adaptin (Affinity Bioreagents), a subunit of the AP2 complex[25]. The cells were then washed extensively with PBS containing 0.2% (w/v) BSA and 0.1% (v/v) triton-X 100 and incubated at room temperature for 30 min with FITC-conjugated goat anti-mouse IgG (Novus Biologicals). The FITC-conjugated antibodies were excited with 488nm Argon-ion laser (Melles Griot) and the fluorescence emission was collected using a 535/50 nm filter. At the laser power used, the emission from EYFP in this detection wavelength range is negligible.

Fluorescence imaging

To obtain a simultaneous image of DiD-labeled viruses and EYFP-tagged clathrin, DiD was excited with a 633 nm helium-neon laser (Melles-Griot) while EYFP was excited with a 532 nm diode-pumped Nd:YAG laser (Crystalaser). A custom designed polychroic beam splitter (Chroma) that reflects at wavelengths 520–550 nm and 615–655 nm was used to direct the laser lines onto the sample. The fluorescent emission from DiD and EYFP was collected by an oil-immersion objective with numerical aperture 1.45 (Olympus), spectrally separated by 610 nm long-pass dichroic mirrors (Chroma) and imaged onto two separate areas of the CCD camera (Roper Scientific, CoolSnap HQ). A 665 long pass filter was used for DiD emission and a 585/70 nm band pass filter was used for EYFP emission. Image series were recorded at 2 frames per second. For co-imaging of DiD-labeled viruses and EGFP-tagged caveolin, a 488 nm argon-ion laser (Melles Griot) was used to excite EGFP. A custom designed polychroic beam splitter (Chroma) that reflects at 475–495 nm and 615–640 nm was used to direct the laser lines onto the sample. Differential interference contrast optics were used to obtain cell images before and after the fluorescence imaging. Experiments were conducted at 37°C unless otherwise mentioned.

Image analysis

Each frame of the DiD fluorescence image series was processed by convolving with a Gaussian spatial filter to remove background and noise. Virus peaks were detected by recursively integrating over bright regions connected to each local maximum. The location of each virus was computed as the centroid of the bright region. Physical trajectories of viruses were reconstructed by pairing peaks in each frame to previously established trajectories according to proximity and similarity in intensity. The EYFP intensity associated with the virus was determined by subtracting a low-spatial frequency background signal in the EYFP channel and

then integrating the EYFP signal weighted by the DiD signal of the virus. Only those viruses that start in the peripheral region of the cell surface and move roughly within the focal plane are analysed. Viruses that move by a substantial amount orthogonal to the focal plane (out of focus) are not considered. As BS-C-1 cells are comparatively flat, most virus trajectories remain close to the focal plane.

Supplementary Material

Refer to Web version on PubMed Central for supplementary material.

Acknowledgments

We thank J. H. Keen and A. Helenius for their generous gifts of GFP-clathrin-LCa and Caveolin-1-EGFP plasmids, respectively. This work is supported in part by a Searle Scholarship, a Beckman Young Investigator award, Office of Naval research and National Science Foundation (to X.Z.). M.J.R. is a National Science Foundation pre-doctoral fellow.

References

1. Matlin KS, Reggio H, Helenius A, Simons K. Infectious entry pathway of influenza-virus in a canine kidney-cell line. J Cell Biol 1981;91:601–613. [PubMed: 7328111]
2. Doxsey SJ, Brodsky FM, Blank GS, Helenius A. Inhibition of endocytosis by anti-clathrin antibody. Cell 1987;50:453–463. [PubMed: 3111717]
3. Anderson HA, Chen YZ, Norkin LC. Bound simian virus 40 translocates to caveolin-enriched membrane domains, and its entry is inhibited by drugs that selectively disrupt caveolae. Mol Biol Cell 1996;7:1825–1834. [PubMed: 8930903]
4. Carbone R, et al. Eps15 and eps15R are essential components of the endocytic pathway. Cancer Res 1997;57:5498–5504. [PubMed: 9407958]
5. Stang E, Kartenbeck J, Parton RG. Major histocompatibility complex class I molecules mediate association of SV40 with caveolae. Mol Biol Cell 1997;8:47–57. [PubMed: 9017594]
6. DeTulle L, Kirchhausen T. The clathrin endocytic pathway in viral infection. EMBO J 1998;17:4585–4593. [PubMed: 9707418]
7. Pelkmans L, Kartenbeck J, Helenius A. Caveolar endocytosis of simian virus 40 reveals a new two-step vesicular-transport pathway to the ER. Nat Cell Biol 2001;3:473–483. [PubMed: 11331875]
8. Sieczkarski SB, Whittaker GR. influenza virus can enter and infect cells in the absence of clathrin-mediated endocytosis. J Virol 2002;76:10455–10464. [PubMed: 12239322]
9. Pelkmans L, Helenius A. Insider information: what viruses tell us about endocytosis. Curr Opin Cell Biol 2003;15:414–422. [PubMed: 12892781]
10. Nichols BJ, Lippincott-Schwartz J. Endocytosis without clathrin coats. Trends Cell Biol 2001;11:406–412. [PubMed: 11567873]
11. Conner SD, Schmid SL. Regulated portals of entry into cells. Nature 2003;422:37–44. [PubMed: 12621426]
12. Brodsky FM, Chen CY, Knuehl C, Towler MC, Wakeham DE. Biological basket weaving: Formation and function of clathrin-coated vesicles. Annu Rev Cell Dev Biol 2001;17:517–568. [PubMed: 11687498]
13. Kirchhausen T. Clathrin. Annu Rev Biochem 2000;69:699–727. [PubMed: 10966473]
14. Nabi IR, Le PU. Caveolae/raft-dependent endocytosis. J Cell Biol 2003;161:673–677. [PubMed: 12771123]
15. Scott MGH, Benmerah A, Muntaner O, Marullo S. Recruitment of activated G protein-coupled receptors to pre-existing clathrin coated pits in living cells. J Biol Chem 2002;277:3552–3559. [PubMed: 11602587]
16. Santini F, Gaidarov I, Keen JH. G protein-coupled receptor/arrestin3 modulation of the endocytic machinery. J Cell Biol 2002;156:556–676.

17. Gaidarov I, Francesca S, Warren RA, Keen JH. Spatial control of coated-pits dynamics in living cells. Nat Cell Biol 1999;1:1–7. [PubMed: 10559856]
18. Skehel JJ, Wiley DC. Receptor binding and membrane fusion in viral entry: the influenza hemagglutinin. Annu Rev Biochem 2000;69:531–569. [PubMed: 10966468]
19. White J, Helenius A, Gething MJ. Heaemagglutinin of influenza virus expressed from a cloned gene promote membrane fusion. Nature 1982;300:658–659. [PubMed: 6815542]
20. Yishimura A, Ohnishi S. Uncoating of influenza viruses in endosomes. J Virol 1984;51:497–504. [PubMed: 6431119]
21. Martin K, Helenius A. Transport of incoming influenza virus nucleocapsids into the nucleus. J Virol 1990;65:232–244. [PubMed: 1985199]
22. Lamb, RA.; Krug, RM. Orthomyxoviridae: the viruses and their replication. In: Knipe, DM.; Howley, PM., editors. Fields Virology. Lippincott Williams and Wilkins; Philadelphia: 2001. p. 1487-1531.
23. Klasse PJ, Bron R, Marsh M. Mechanisms of enveloped virus entry into animal cells. Adv Drug Del Rev 1998;34:65–91.
24. Helenius A, Kartenbeck J, Simon K, Fries E. On the entry of Semliki Forest viruses into BHK-21 cells. J Cell Biol 1980;84:404–420. [PubMed: 6991511]
25. Marrifield CJ, Feldman ME, Wan L, Almers W. Imaging actin and dynamin recruitment during invagination of single clathrin-coated pits. Nat Cell Biol 2002;4:691–698. [PubMed: 12198492]
26. Volonte D, Galbiati F, Lisanti MP. Visualization of cavelin-1, a caveolar marker protein, in living cells using green fluorescent protein (GFP) chimeras. FEBS Lett 1999;445:431–439. [PubMed: 10094502]
27. Wu X, et al. Clathrin exchange during clathrin-mediated endocytosis. J Cell Biol 2001;155:291–300. [PubMed: 11604424]
28. Rappoport JZ, Simon SM. Clathrin-mediated endocytosis during cell migration. J Cell Sci 2003;116:847–855. [PubMed: 12571282]
29. Pelkmans L, Punterner D, Helenius A. Local actin polymerization and dynamin recruitment in SV-40-induced internalization of caveolae. Science 2002;296:535–539. [PubMed: 11964480]
30. Thomsen P, Roepstorff K, Stahlhut M, Deurs BV. Caveolar are highly immobile plasma membrane microdomains, which are not involved in constitutive endocytic trafficking. Mol Biol Cell 2002;13:238–250. [PubMed: 11809836]
31. Schnitzer JE, Oh P, Pinney E, Allard J. Filipin-sensitive caveolae-mediated transport in endothelium-reduced transcytosis, scavenger endocytosis, and capillary-permeability of select macromolecules. J Cell Biol 1994;127:1217–1232. [PubMed: 7525606]
32. Georgi A, Mottola-hartshorn C, Warner W, Fields B, Chen LB. Detection of individual fluorescently labelled reovirions in living cells. Proc Natl Acad Sci USA 1990;87:6579–6583. [PubMed: 2118653]
33. Suomalainen M, et al. Microtubule-dependent plus- and minus end-directed motilities are competing processes for nuclear targeting of adenovirus. J Cell Biol 1999;144:657–672. [PubMed: 10037788]
34. Seisenberger G, et al. Real-time single-molecule imaging of the infection pathway of an Adeno-associated virus. Science 2001;294:1929–1932. [PubMed: 11729319]
35. McDonald D, et al. Visualization of the intracellular behavior of HIV in living cells. J Cell Biol 2002;159:441–452. [PubMed: 12417576]
36. Lakadamyali M, Rust MJ, Babcock HP, Zhuang X. Visualizing infection of individual influenza viruses. Proc Natl Acad Sci, USA 2003;100:9280–9285. [PubMed: 12883000]
37. Wagner R, Matrosovich M, Klenk H-D. Functional balance between haemagglutinin and neuraminidase in influenza virus infection. Rev Med Viol 2002;12:159–166.
38. Babu YS, et al. BCX-1812 (RWJ-270201): Discovery of a novel, highly potent, orally active, and selective influenza neuraminidase inhibitor through structure-based drug design. J Med Chem 2000;43:3482–3486. [PubMed: 11000002]
39. Sidwell RW, et al. In vivo influenza virus-inhibitory effects of the cyclopentane neuraminidase inhibitor RWJ-270201. Antimicrob Agents Chemo 2001;45:749–757.
40. Rothberg KG, Ying YS, Kamen BA, Anderson RGW. Cholesterol controls the clustering of the glycophospholipid-anchored membrane-receptor for 5-methyltetrahydrofolate. J Cell Biol 1990;111:2931–2938. [PubMed: 2148564]

41. Naslavsky N, Weigert R, Donaldson JG. Convergence of non-clathrin-and clathrin-derived endosomes involves Arf6 inactivation and changes in phosphoinositides. Mol Biol Cell 2003;14:417–431. [PubMed: 12589044]

42. Sieczkarski SB, Whittaker GR. Differential requirements of Rab5 and Rab7 for endocytosis of influenza and other enveloped viruses. Traffic 2003;4:333–343. [PubMed: 12713661]

43. Connolly JL, Green SA, Greene LA. Pit formation and rapid changes in surface morphology of sympathetic neurons in response to nerve growth factors. J Cell Biol 1981;90:176–180. [PubMed: 7251673]

44. Wilde A, et al. EGF receptor signaling stimulates SRC kinase phosphorylation of clathrin, influencing clathrin redistribution and EGF uptake. Cell 1999;96:677–687. [PubMed: 10089883]

45. Grimes ML, et al. Endocytosis of activated TrkA: Evidence that nerve growth factor induces formation of signaling endosomes. J Neuro 1996;16:7950–7964.

46. Beattie EC, Howe CL, Wilde A, Brodsky FM, Mobley WC. NGF signals through TrkA to increase clathrin at the plasma membrane and enhance clathrin mediated membrane trafficking. J Neuro 2000;20:7325–7333.

47. Peter BJ, et al. BAR domains as sensors of membrane curvature: the amphiphysin BAR structure. Science 2004;303:495–499. [PubMed: 14645856]

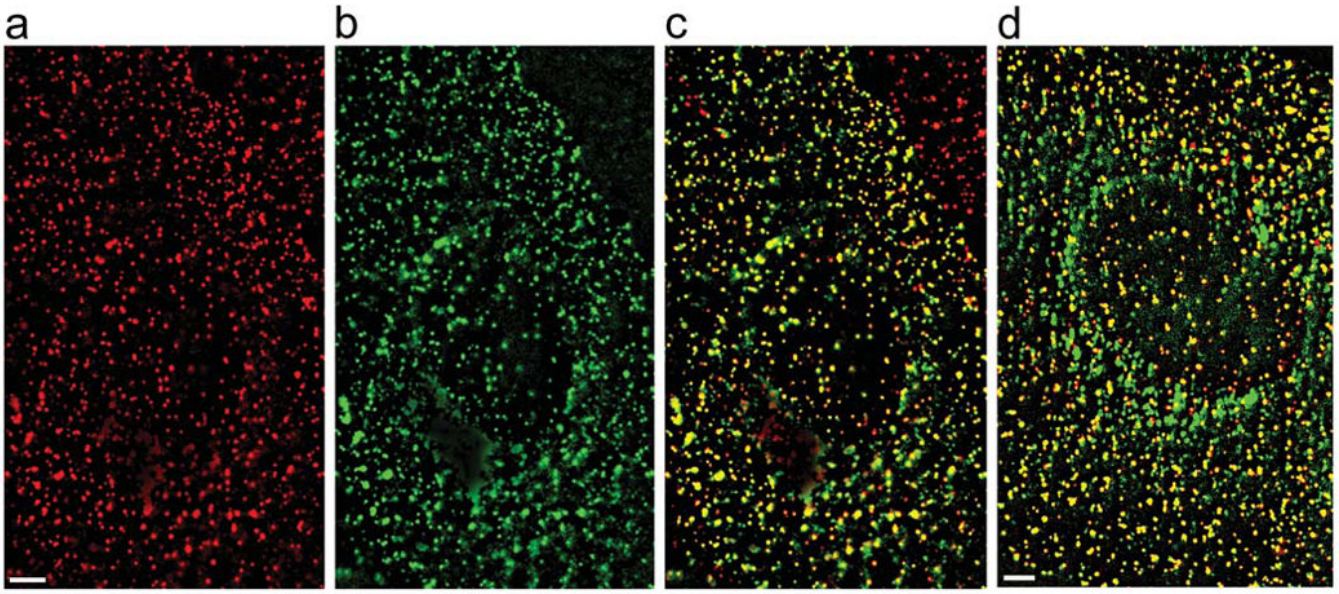

Figure 1.

Fluorescence images of clathrin-coated structures in BS-C-1 cells expressing EYFP-clathrin. For a clearer visualization of discrete fluorescent spots, a low-spatial frequency background due to cytoplasmic EYFP-clathrin has been subtracted from the images. Scale bars: 3 μm (**a**) The immunofluorescence image of clathrin-coated structures in a cell transiently transfected with EYFP-clathrin. (**b**) The EYFP fluorescence image of clathrin-coated structures in the same cell. (**c**) Overlay of the immunofluorescence signal (red) with the EYFP signal (green). Pixels with both red and green signal appear yellow. Counting spots in multiple cells shows that over 97% of the clathrin-coated structures that appeared in the immunofluorescence image colocalized with those in the EYFP image. The red-only spots in the upper-right corner of the image belong to a neighboring cell not transfected with EYFP-clathrin. (**d**) Overlay of the transferrin image (red) and EYFP image (green) of a cell stably expressing EYFP-clathrin. Alexa Fluor 647-labeled transferrin (Molecular Probes) was bound to cells at 4°C for 15 minutes. After removing unbound transferrin, cells were imaged at room temperature. An image of the first 5 s is shown. Over 96% of the transferrin spots colocalize with clathrin-coated structures and appear yellow.

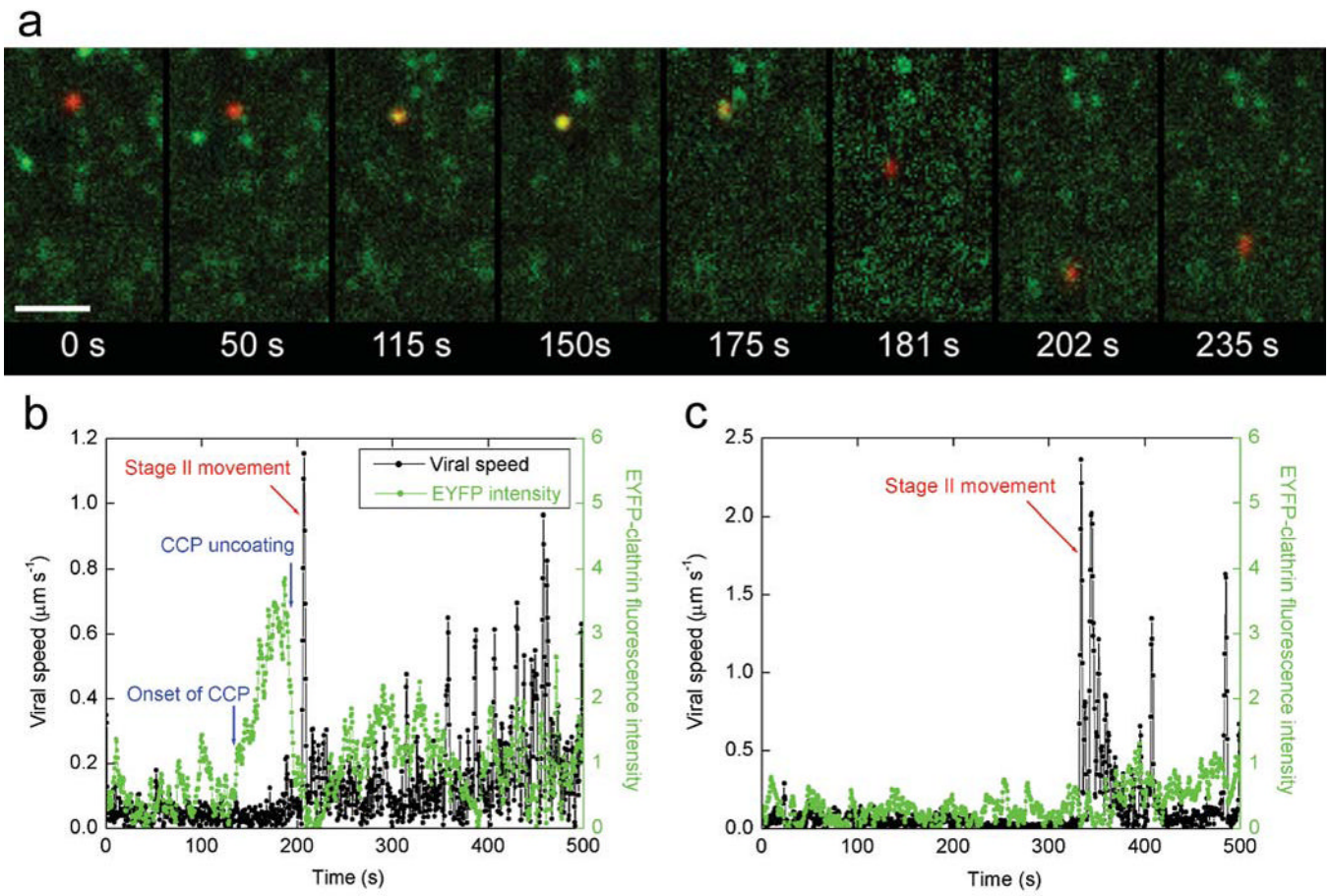

Figure 2.

Internalization of influenza viruses via multiple pathways. (**a**) Snapshots of a virus internalized via a CCP. A live movie of this virus is available as **Supplementary Video 3**. Scale bar: 10 μm. t = 0 s: the virus (red) binds to the cell. t = 50 s: the virus is undergoing stage I movement. t = 115 s: a CCP labeled with EYFP (green) begins to form at the virus site. t = 150 s, the clathrin coat reaches its peak fluorescence intensity. t = 175 s: the clathrin coat rapidly disassembles. t = 181 seconds: the virus is transported towards the nucleus on a microtubule (stage II movement). t = 202 s: the virus enters stage III transport involving both plus- and minus-ended-directed motilities on microtubules. t = 235 s: the virus continues stage III movement. (**b**) The time-trajectories of a virus internalized via *de novo* formation of a CCP. Black symbols are the velocity time-trajectories of the virus. Stage II movement is identified as the rapid unidirectional translocation from the cell periphery to the perinuclear region (red arrows). Green symbols are the integrated fluorescence intensity of EYFP-clathrin associated with the virus. (**c**) The time-trajectories of a virus internalized without association with a clathrin-coated structure. Symbols are as defined in **b**. Live movies of the two viruses in **b** and **c** are also available (**Supplementary Videos 4 and 5**).

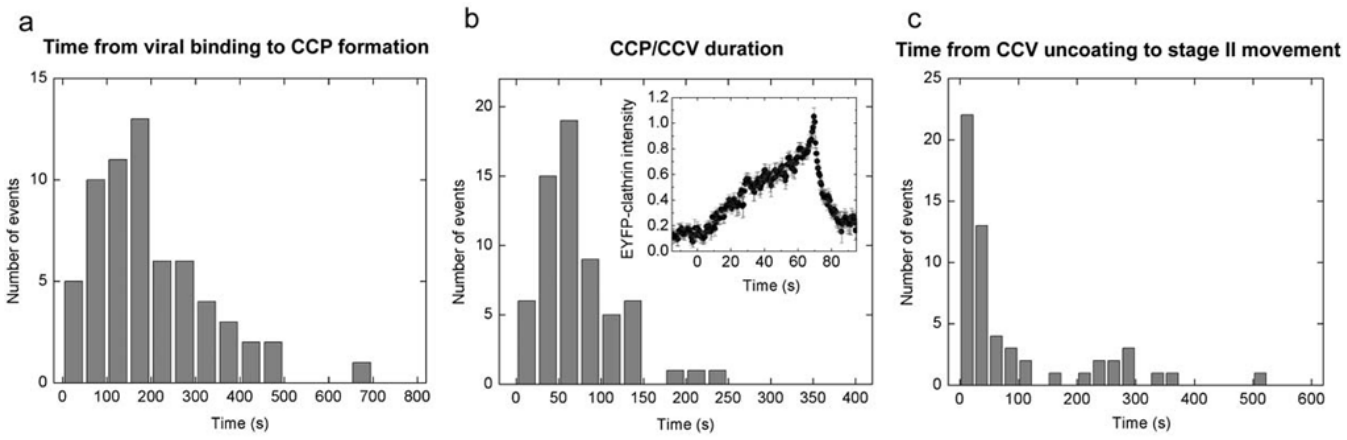

Figure 3.

Dynamics of the CCPs and CCVs formed *de novo* at the virus-binding sites. (**a**) A histogram of the time between viral binding and onset of CCP formation. (**b**) A histogram of the time between the onset of CCP formation and CCV uncoating. Inset: an averaged curve of 60 time-trajectories of the EYFP-clathrin intensity associated with viruses shows the life cycle of CCPs. Each EYFP-clathrin trajectory was normalized to the peak height and scaled in time so that the onset of the CCP formation occurs at t = 0 sec and the peak clathrin intensity occurs at t = 69 sec, which is the average duration of the clathrin-accumulation phase. (**c**) A histogram of the time between the first CCV uncoating event and the onset of stage II viral movement.

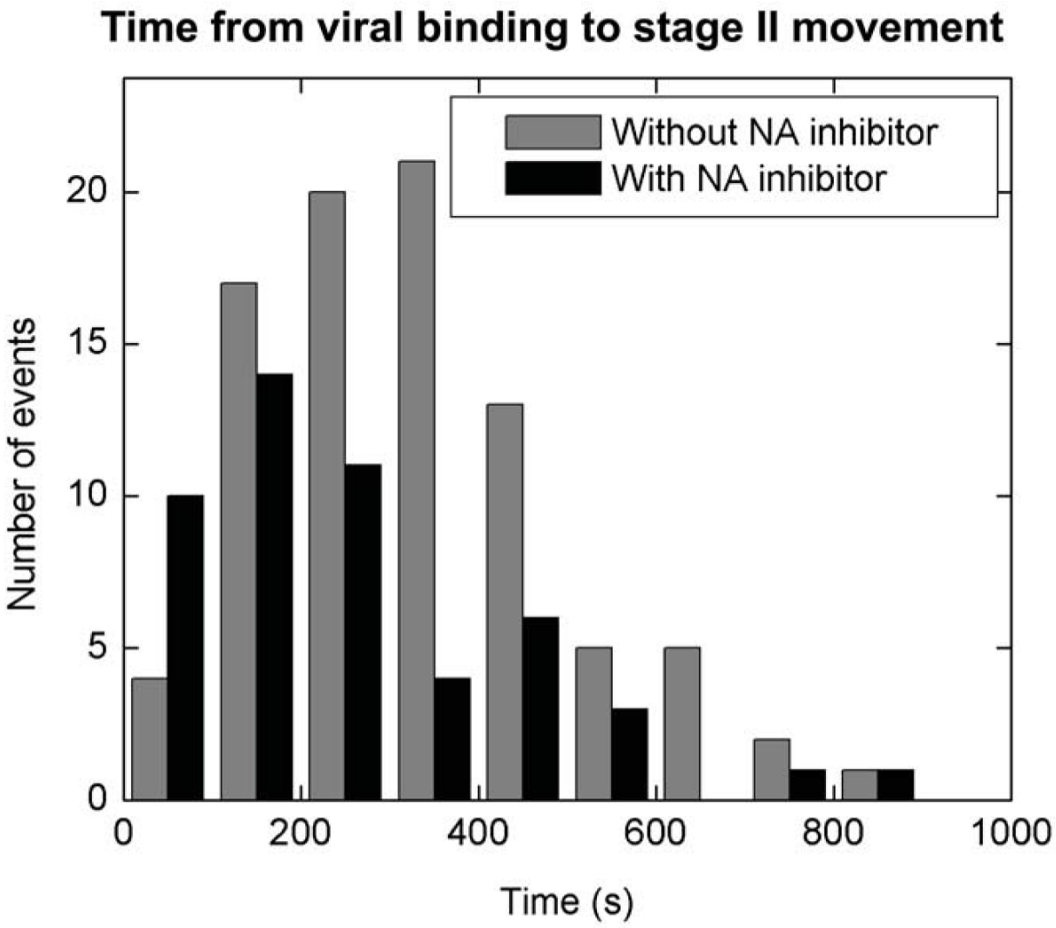

Figure 4.
The effect of neuraminidase (NA) inhibitors on the endocytosis of influenza viruses. Grey columns show a histogram of the time between viral binding and the onset of stage II movement in the absence of neuraminidase inhibitors. Red columns show the histogram in the presence of 1 μM RWJ270201. The histogram in the presence of 1 μM oseltamivir is similar (data not shown).

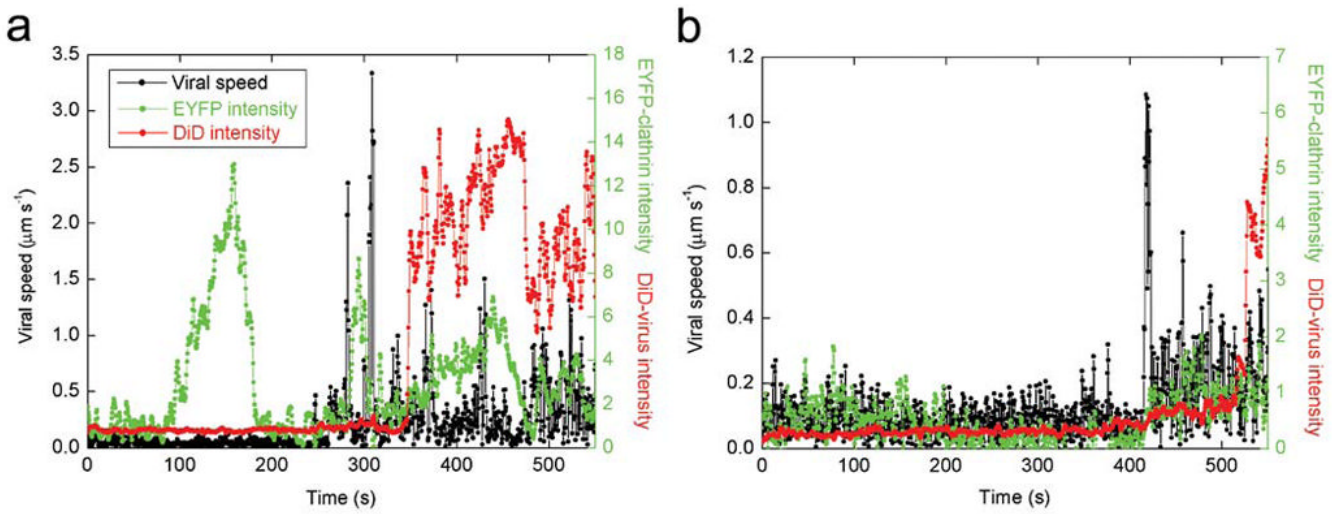

Figure 5.

Time-trajectories of viruses that successfully fused after endocytosis. (**a**) An example of a virus that was internalized via a CCP. (**b**) An example that was internalized without association with a CCP. Live movies of these two viruses are available (**Supplementary Videos 6 and 7**). Black symbols are the velocity time-trajectories of the viruses. Red symbols are the integrated DiD fluorescence intensities of the viruses. Viral fusion can be identified as a dramatic increase of the DiD signal. Green symbols are the integrated fluorescence intensities of EYFP-clathrin associated with the viruses.